

Article

Study on the Dynamic Responses of a Large Caisson during Wet-Towing Transportation

Haoyang Gu ¹, Huakun Wang ^{1,*}, Qiu Zhai ¹, Weibing Feng ¹ and Jiaxiu Cao ²

¹ College of Harbor, Coastal and Offshore Engineering, Hohai University, Nanjing 210098, China; hhughy@hhu.edu.cn (H.G.); zq431@hhu.edu.cn (Q.Z.); wbfeng@hhu.edu.cn (W.F.)

² School of Naval Architecture & Ocean Engineering, Jiangsu University of Science and Technology, Zhenjiang 212003, China; 13961502826@163.com

* Correspondence: hkwang@hhu.edu.cn

Abstract: Large caissons are extensively applied as deep-water foundations in marine engineering. In fact, caissons are generally prefabricated and transported to project site by wet towing. Motion responses of large caissons and those occurring during the towing process were investigated, and CO₂ emissions under various conditions were calculated. These are all considered to ensure towing safety and environmental protection. The caisson resistance coefficient was simulated via Ansys Fluent software. The effects of towrope length, towing speed, and drift depth on the motion responses of caissons under the combined action of wind and wave were evaluated via Ansys AQWA software. Maximum heave value was dominantly affected by rope length and draft depth, and its fluctuation was highly influenced by towing speed and draft depth. However, all of the above mentioned factors had insignificant influences on pitch response. When towing existed, rope tension was rapidly increased from zero to a constant value that depended on towing speed and drift depth. However, the speed of achieving this stable phase depended on the length of the towrope.

Keywords: large caissons; wet-towing; stability; dynamic response; towrope tension



Citation: Gu, H.; Wang, H.; Zhai, Q.; Feng, W.; Cao, J. Study on the Dynamic Responses of a Large Caisson during Wet-Towing Transportation. *Water* **2021**, *13*, 126. <https://doi.org/10.3390/w13020126>

Received: 24 November 2020

Accepted: 4 January 2021

Published: 7 January 2021

Publisher's Note: MDPI stays neutral with regard to jurisdictional claims in published maps and institutional affiliations.



Copyright: © 2021 by the authors. Licensee MDPI, Basel, Switzerland. This article is an open access article distributed under the terms and conditions of the Creative Commons Attribution (CC BY) license (<https://creativecommons.org/licenses/by/4.0/>).

1. Introduction

To response to the requirements of today's globalized world, oceanographic engineering has rapidly progressed [1]. In addition, caissons have been extensively applied in offshore structures such as wind turbines, cross-sea bridges, and gas and oil platforms. Today, high quality onshore caissons are first constructed, wet-towed with a small tugboat to project site, and installed on the seabed via a water-displacement self-sinking method. Towing operations have been performed for several years as an inexpensive transportation method for a great quantity of commodities [2]. Kim et al. compared the costs of wet and dry towing methods for a semisubmersible platform. The obtained results showed that wet towing was the cheapest option for their project [3,4]. However, in some environments, such as port, open sea, coastal waters, and internal waters, water towing operations may be the only choice. Each of the abovementioned environments have a variety of potential hazards [5]. In addition, regardless of planning feasibility, accidents can take place in towing operations, even in mild weather, inflicting enormous casualties and economical losses [6–8]. Hence, accurate studies have to be conducted to address the requirement of wet towing operations and ensure the practicability of the developed integrated transportation method.

Towing operations, which include the transportation of self-floating objects using one or more towing tugs, are very common in ocean engineering projects [9]. Towing dynamics are very similar to those of moored objects in currents [5]. In recent years, several authors, some of whom have applied traditional theoretical methods, have investigated this topic. Bernitsas and Kekridis [10] proposed a 3-Degrees of Freedom (3-DOF) fully analytical model for the investigation of the towing stabilities of some vessels towed by

elastic towlines. They derived a formulation for the determination of dynamic system equilibria and employed Routh–Hurwitz criterion for the evaluation of towing stability. They also evaluated the influence of the variations of maneuvering derivatives on equilibrium stability through sensitivity analyses. [11] investigated Jacobian matrix eigenvalues of dynamic systems. [12,13] developed a model for analyzing tug-barge system course stability based on a classical non-linear derivative-based method. The towline was assumed to be a two-dimensional (2D) lumped-mass line. Their results revealed that longer towing lines decreased unfavorable influences due to the slewing motion on the tug. Their model, in which the influence of wind was taken into account, detected stable regions of the course for the towed barge based on the angle of the wind encountered at various speeds of wind and the length of towing line.

Numerical analysis methods have also been applied by various researchers. Several wet tow operations were investigated, most of which were related to offshore wind turbines and nuclear plants. These authors have generally focused on key influencing factors and the stability features of towing [14]. Towing motion behaviors of jack-up [15] and multi-cylinder Floating Production, Storage and Offloading unit (FPSO) [16] units under different towing conditions were investigated for the estimation of extreme motions. [17] studied floating wind turbine stability and simulated towline force using SESAM [18] applied MOSES for the investigation of offshore integrated meteorological mast (OIMM) stability while performing wet towing. The obtained results revealed that both mooring position and draft depth greatly affected dynamic response. However, researchers have generally neglected towrope tension during towing; in other words, they have neglected towing feasibility and safety.

A great number of research works have been performed on simulating offshore structures. However, few researchers have numerically studied the transportation of large non-streamlined structures by wet-tow. In addition, few researchers have considered the environmental impact of air emissions from the project. In the current work, an economic towing procedure consisting of tugboats, a polyester fiber towrope, and a large caisson has been developed. Dynamic response and static stability due to the combination of wind and wave were simulated using Ansys AQWA (Ansys, Shanghai, China). Towrope tension and air emissions have also been evaluated to guarantee towing scheme feasibility and safety and to ensure that practices are environmentally friendly.

2. Caisson Model and Towing System

2.1. Caisson Model

The caisson investigated in the current work was a reinforced concrete frame structure used in the construction of a bridge with a length of 69 m, a width of 44 m, and a height of 16.8 m. Figure 1a shows the top view of the caisson structure graphing. The thicknesses of the outside and inside walls were 450 and 300 mm, respectively. Due to the design and installation requirements of the superstructures, the inner walls were 3 m shorter than the outer ones. Figure 1b shows the three-dimensional (3D) model of the simulated caisson using Ansys SpaceClaim (Ansys, Shanghai, China). More details and parameter values are summarized in Table 1. Initial draft meant that, at draft value of 8.2 m, buoyancy was equal to its self-weight. The caisson compartments were filled during wet towing. Therefore, the applied drift could be adjusted to meet safety requirements. The towing operation was performed in the Yellow Sea of China under the following sea conditions: wave period, 6.1 s; wave height, 1m; and wind speed, 6 m/s.

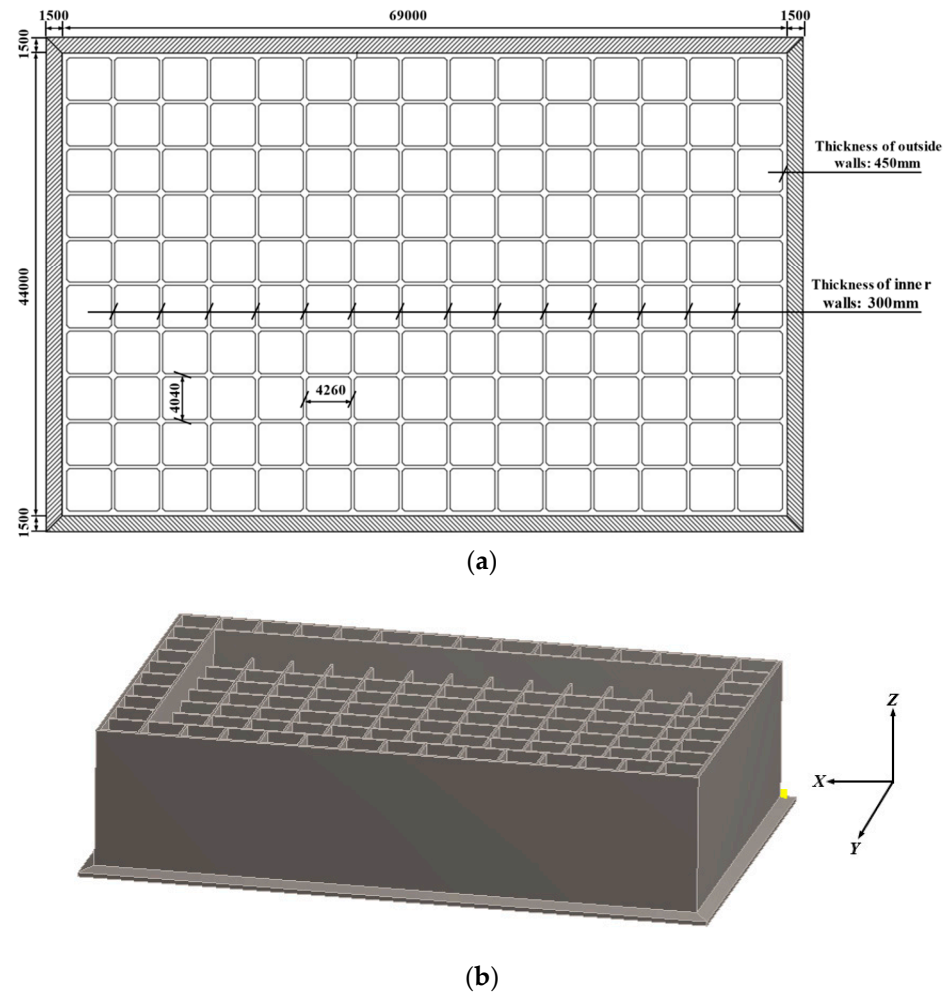


Figure 1. (a) Top view of the caisson; (b) Caisson model simulated in Ansys SpaceClaim.

Table 1. Main parameters of caisson.

Items	Value
Length/m	69
Width/m	44
Height/m	16.8
Initial draft/m	8.2
Center of gravity/m	(0, 0, 5.58)
Radius of gyration (COG)/m	(5, 7, 8)

2.2. Towing System

In the current study, the towing system consisted of a tug boat, towing rope, and caisson and was simulated using Ansys software (Figure 2). Both global and local coordinate systems were applied. The tug boat and caisson were modeled in a local coordinate system, and the towing operation was simulated by Ansys AQWA. The towing rope was made of a mix of steel wire with a large diameter, produced by JIAN FENG SLING CO., LTD (Guangzhou, China) [19], and its cross-section is shown in Figure 3. It should be noted that, because only one towrope was used in the towing process, at high towing speeds, multiple tugs might need to be tied to the end of the towrope to provide enough power. However, when studying the dynamic responses of the caisson, we simplified the model and assumed that it was towed by one tugboat.

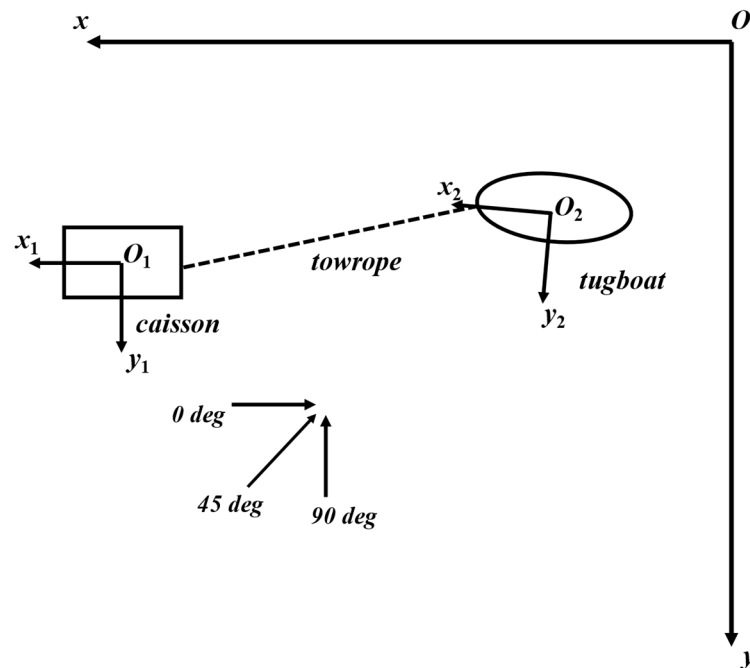


Figure 2. Coordinate systems applied in the research.

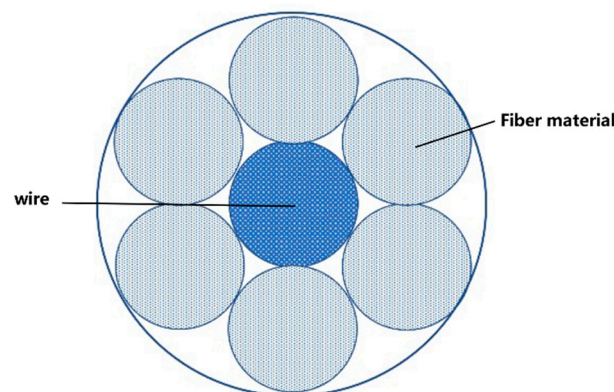


Figure 3. Cross-section of towing rope.

3. Numerical Method

3.1. Intact Stability Analysis

Metacentric height (GM) is an essential key parameter for the measurement of floating structure initial static stability, and this was calculated as the distance from the gravity center to the metacenter. Higher metacentric values indicated favorable initial stabilities against overturning. Sometimes the height of the metacentric also reflects the rolling model frequency of the structure [20]. In the current work, metacentric height was obtained by:

$$GM = BM - (Z_g - Z_b) \tag{1}$$

$$BM = \frac{I}{\nabla} \tag{2}$$

where BM is the metacentric radius obtained as distance from buoyancy center to metacenter, ∇ is displacement volume, I is inertia moment from floating structure waterplane to axis, Z_B is buoyancy center, and Z_G is gravity center.

3.2. Hydrodynamics Analysis

Wind, currents, and waves are the three key factors affecting the stability of the floating structure during wet towing. Hence, the responses of the structures in different environments is a great problem that has been solved in this work. The main goal of this study was to provide proper insight into practical applications such as offshore structure design, installation plans, and transportation formulation. The time histories of caisson motion with six degrees of freedom (6-DOF) were stated in the reference system by adopting the water plane as the origin. Based on 3D potential theory, hydrodynamic moments and forces on the caisson were obtained.

The dynamic equation for a floating body under various complex loadings is stated as:

$$[M + \Delta M]\ddot{X} + [B_{rad} + B_{vis}]\dot{X} + [K_{stillwater} + K_{mooring}]X = F_1 + F_{2Low} + F_{2High} + F_{wind} + F_{current} + F_{others} \tag{3}$$

where M is floating body mass matrix, ΔM is floating body added mass matrix, B_{vis} is viscous damping matrix, B_{rad} is radiation damping matrix, $K_{stillwater}$ is hydrostatic stiffness matrix, $K_{mooring}$ is mooring system stiffness matrix, F_1 is first order frequency load matrix, F_{2Low} is second order low frequency load matrix, F_{2High} is second order high frequency load matrix, F_{wind} is wind load matrix, $F_{current}$ is current load matrix, and F_{others} is the remaining load matrix. Floating body mass matrix is stated as:

$$M_{ij} = \begin{bmatrix} M & 0 & 0 & 0 & Mz_G & -My_G \\ 0 & M & 0 & -Mz_G & 0 & Mx_G \\ 0 & 0 & M & My_G & -Mx_G & 0 \\ 0 & -Mz_G & My_G & I_{xx} & I_{xy} & I_{xz} \\ Mz_G & 0 & -Mx_G & I_{yx} & I_{yy} & I_{yz} \\ -My_G & Mx_G & 0 & I_{zx} & I_{zy} & I_{zz} \end{bmatrix} \tag{4}$$

where (x_G, y_G, z_G) is gravity center position and I_{ij} is inertia mass.

Hydrostatic stiffness matrix is stated as:

$$K_{ij,stillwater} = \begin{bmatrix} 0 & 0 & 0 & 0 & 0 & 0 \\ 0 & 0 & 0 & 0 & 0 & 0 \\ 0 & 0 & \rho g S & \rho g S_2 & -\rho g S_1 & 0 \\ 0 & 0 & \rho g S_2 & \rho g(S_{22} + Vz_B) - Mgz_G & -\rho g S_{12} & -\rho g Vx_B + Mgx_G \\ 0 & 0 & \rho g S_1 & -\rho g S_{12} & \rho g(S_{11} + Vz_B) - Mgz_G & -\rho g Vy_B + Mgy_G \\ 0 & 0 & 0 & -\rho g Vx_B + Mgx_G & -\rho g Vy_B + Mgy_G & 0 \end{bmatrix} \tag{5}$$

where (X_B, Y_B, Z_B) is buoyancy center position, S is water plane area, and S_i and S_{ij} are the first and second order moments of the water plane area.

In the current work, ΔM , B_{rad} , F_1 , F_{2Low} , and F_{2High} are obtained by AQWA-Line software and B_{vis} is determined by Morison theory. Wind and current drag were obtained in a similar way. Environment load coefficients are defined as:

$$C = \frac{2F}{Av^2} \tag{6}$$

where F is drag force, A is the area of body incident to flow, and v is velocity relative to wind or current positions.

Therefore, force is determined as:

$$F = \frac{1}{2}CAv^2 \tag{7}$$

In the current work, load coefficients have been determined using Ansys Fluent software. Figure 4 shows the computational domain obtained based on the findings of Lee et al. [21] and Liu et al. [22]. Fore body was 1.5 L away from the velocity inlet and aft body was 2.5 L away from the pressure outlet. In addition, lateral distance between

wall and body was $2L$. First-order temporal and second-order convection schemes were applied for temporal and momentum equations, respectively, to be applied to perform spatial discretization. Jin et al. [23] and He et al. [24] applied the $k - \omega$ Shear Stress Transfer (SST) turbulence model to analyze the Reynolds averaged Navier-Stokes (RANS) equation and obtained satisfactory results. In the current work, the $k - \omega$ SST turbulence model was also applied.

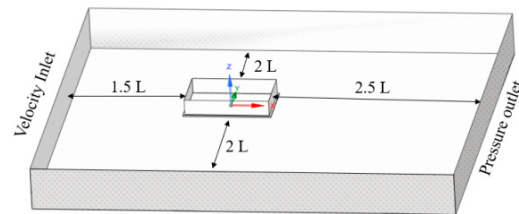


Figure 4. Computational domain in Ansys Fluent.

For the verification of the accuracy of the developed method, square cylinder load coefficients applied in the Tang's [25] experimental research were obtained, and the obtained results are summarized in Table 2. The result errors of the two methods were lower than 5%, which meant that the developed numerical method could effectively calculate load coefficients. Environment load coefficients of the investigated caisson are shown in Figure 5.

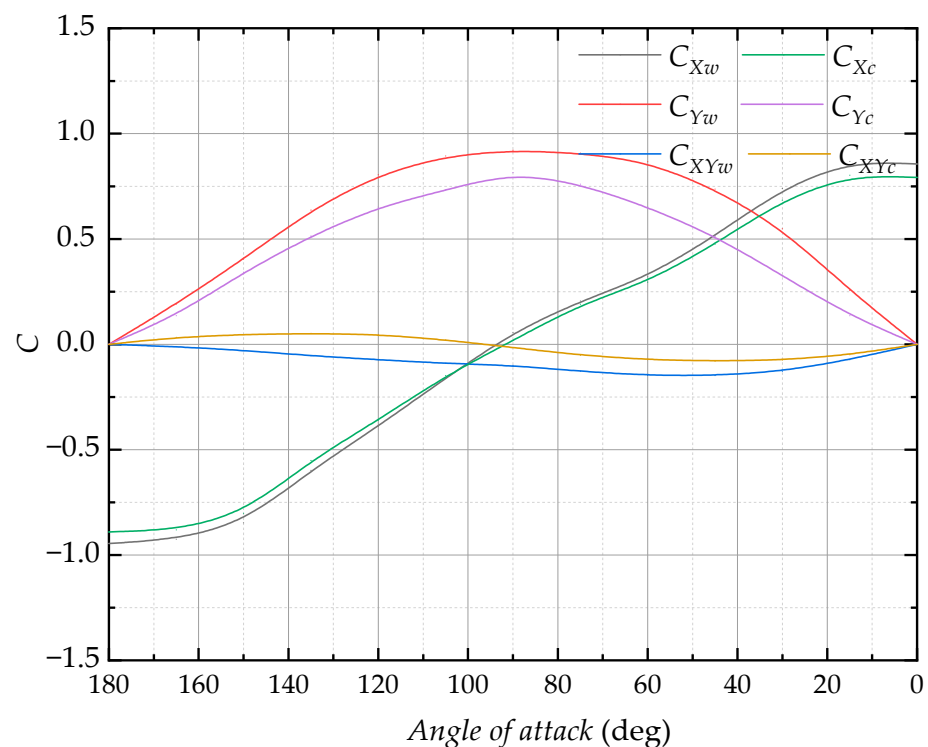


Figure 5. Environment load coefficients.

Table 2. Load coefficients calculated by Tang and Fluent.

Angle/deg	C _{Tang's}	C _{fluent}	Error
0	1.88	1.931	2.71%
10	1.26	1.294	2.70%
20	1.26	1.276	1.27%
30	1.33	1.351	1.58%
45	1.42	1.464	3.10%

The Joint North Sea Wave Project (JONSWAP) spectrum was applied as the wave spectrum. Empirical parameters γ and α , as well as peak frequency, were also applied. Spectral ordinate at any frequency is stated as:

$$S(\omega) = \frac{\alpha g^2 \gamma^\alpha}{\omega^5} \exp\left(-\frac{5\omega_p^4}{4\omega^4}\right) \quad (8)$$

where ω_p is peak frequency, γ is peak enhancement factor, and α is a constant value that depends on wave spectrum peak frequency and wind speed, which can be determined as:

$$\alpha = \exp\left(-\frac{(\omega - \omega_p)^2}{2\sigma^2 \omega_p^2}\right) \quad (9)$$

$$\sigma = \begin{cases} 0.07 & \text{where } \omega \leq \omega_p \\ 0.09 & \text{where } \omega > \omega_p \end{cases}$$

Starting and finishing frequencies are also expressed as:

$$\omega_s = \omega_p \left(0.58 + 0.05 \frac{\gamma - 1}{19}\right) \quad (10)$$

$$\omega_f = F(\gamma) \cdot \omega_p \quad (11)$$

where $F(\gamma)$ is a weighting function, and weighting function values against $\gamma \in [1.0, 20.0]$ are available in the AQWA Theory Manual.

3.3. Mesh Convergence Analyses

The analysis of mesh density had to be performed when calculating mean wave drift moments and forces on the structure using both Pinkster (near-field) and Maruo-Newman (far-field) methods to obtain optimum accuracy and efficiency. Mesh size had to be smaller than both one seventh of the wave length size and the minimum dimensional feature of the caisson. A full-sized caisson model was developed with mesh sizes of 0.8, 1.0, 1.2, and 1.5 m. Mean wave drift moments and forces obtained from the two methods were compared. All parameters except element size were the same when using both models. The obtained results are shown in Figure 6.

As can be seen from Figure 6, the mean wave drift moments and forces obtained by the various methods were almost the same at time periods longer than 20 s. However, at periods of less than 20 s, the findings of the two methods were different. Finally, at a mesh size of 1 m, the results obtained from the two methods were similar. Based on the abovementioned findings, a 1 m mesh size was adopted in this analysis.

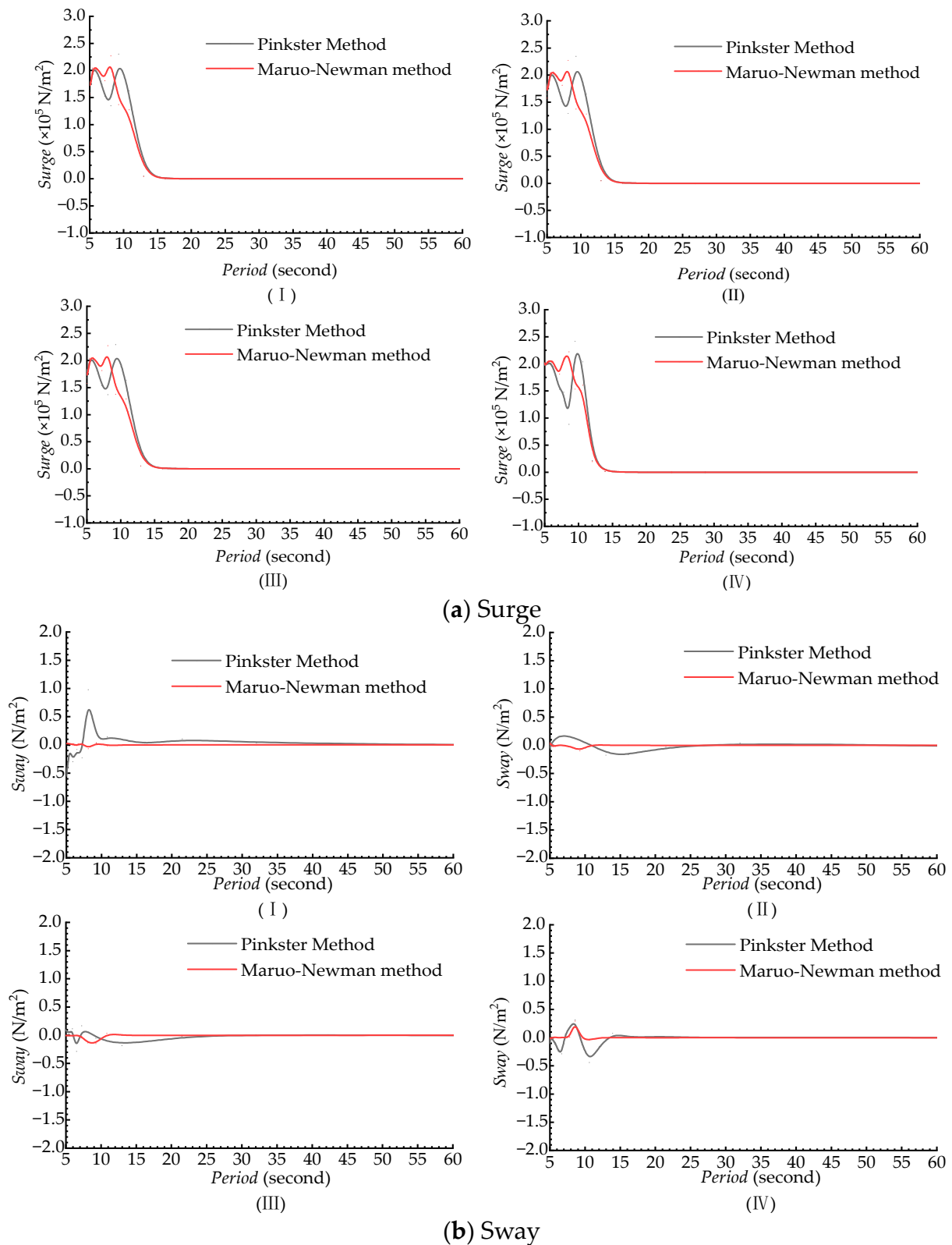


Figure 6. Cont.

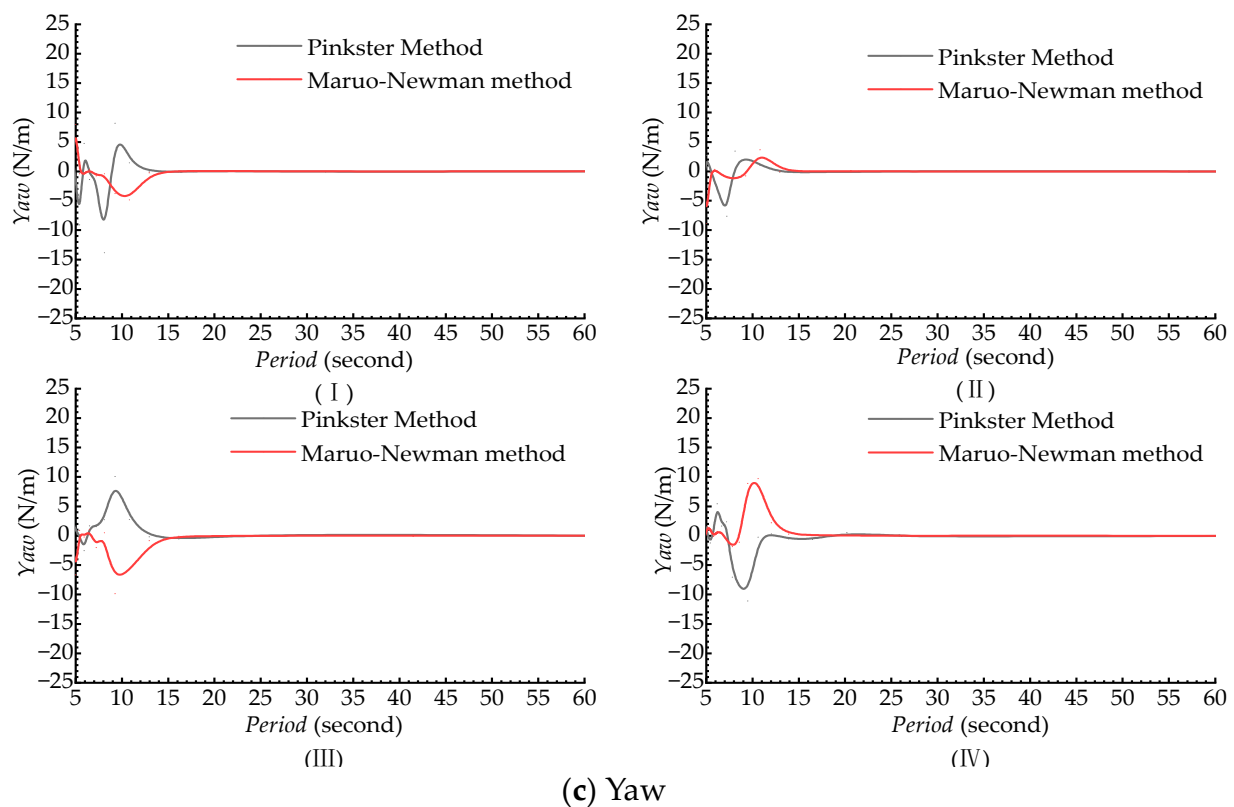


Figure 6. Mean wave drift forces and moments on the structure. Note: (I) mesh size, 0.8 m; (II) mesh size, 1.0 m; (III) mesh size, 1.2 m; (IV) mesh size, 1.5 m.

3.4. Estimation of CO₂ Emissions

Currently, an increasing number of engineering projects are required to take proper measures regarding air emissions due to global warming. In this study, we also estimated CO₂ emissions during towing. It was assumed from experience that a tugboat could provide a pulling force of 199.92 kN/1000 kW. We then calculated the number of required tugboats based on rope tension. Emissions were estimated according to the following formula [26]:

$$\text{Emissions} = \text{MCR} \times \text{LF} \times A \times \text{EF} \quad (12)$$

where *MCR* is the maximum continuous of the combustion engine in use, kW; *LF* is the engine load factor during specific activity; *A* is activity time, h; and *EF* is emissions factor, kg/kWh.

4. Numerical Results

4.1. Stability Analysis Results

Intact stability parameters of the caisson were calculated using theoretical and numerical simulation methods, and the obtained results are shown in Table 3. From the data given in the table, it was found that the difference of *GM* obtained by the two methods was less than 5%. Additionally, the *GM* value was decreased by increasing drift, which agreed with the findings of Rawson [20], reported in his book. All above conclusions proved the accuracy and feasibility of the developed numerical method.

The caisson frequency domain was also analyzed. Figure 7 shows caisson's response amplitude operators (RAOs) for a wave direction of 0 degrees. First-order wave frequency was about 0.5–0.8 rad/s. As the drift increases, the peak of RAOs increases accordingly. The above findings lay a solid foundation for follow-up time domain analysis.

Table 3. Parameters calculated by theoretical method and numerical simulation.

Drift/m	-	I_{XX}/m^4	∇/m^3	BM/m	Z_B/m	Z_G/m	GM/m	Error
11.50	AQWA	489,807.00	35,122.00	13.95	−5.79	−6.76	14.92	4.65%
11.50	Theoretical	506,950.25	34,914.00	14.52	−5.79	−6.91	15.64	
12.50	AQWA	489,807.00	38,209.40	12.82	−6.29	−7.66	14.19	3.82%
12.50	Theoretical	506,950.25	37,950.00	13.36	−6.29	−7.68	14.75	
13.50	AQWA	489,807.00	41,247.10	11.87	−6.79	−8.50	13.58	4.28%
13.50	Theoretical	506,950.25	40,986.00	12.37	−6.79	−8.61	14.19	

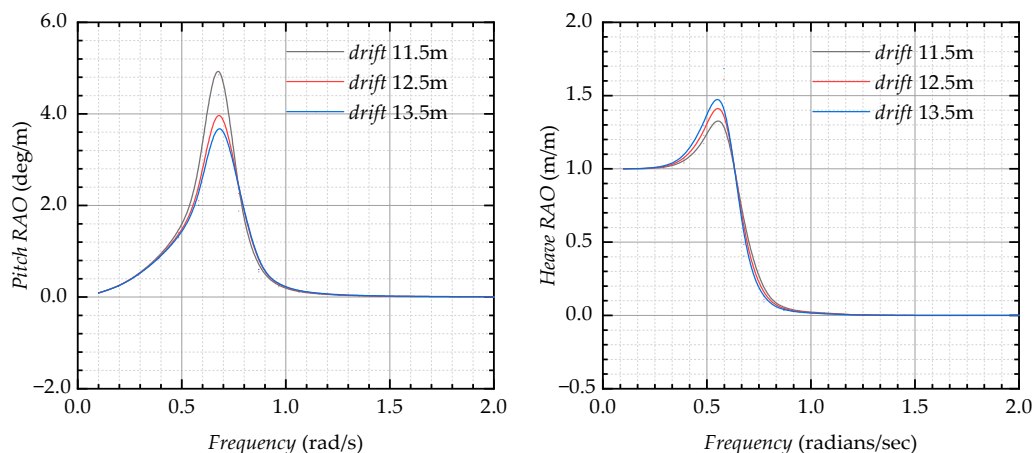


Figure 7. Pitch and Heave RAOs.

4.2. Results of Dynamic Response

Towing float hydrodynamic responses rely on many factors such as sea load conditions and drafts as well as towing system parameters such as tow speed, towrope length, etc., and a safe towing plan can be easily developed by analyzing the influences of various factors on the dynamic responses. Random sea conditions according to a JONSWAP spectrum with high corresponding frequency and wave height were applied in this work. On the basis of the real sea conditions of a towing project, wave height and frequency values of 1 m and 1.03 rad/s, respectively, were adopted in this work. Wind was assumed to be a steady flow with a speed of 6 m/s.

In the time-domain analysis, three different drift values were evaluated. The statistical values of two time durations of 1 and 3 h are summarized in Tables 4 and 5, respectively. According to the literature [27] maximum pitch and heave values were normalized to perform deeper comparison. Normalized values are obtained as:

$$Normalized \ Max = \frac{Max - Mean}{STD} \tag{13}$$

where *Max* is maximum value in the whole process, *Mean* is arithmetic mean value, and *STD* is standard deviation.

As seen in Table 4, *STD* and normalized max. error were generally less than 10% for different simulation times, and mean value barely changed. From Table 5, it is shown that caisson pitch for various simulation times also presented the same variation trend. Figures 8 and 9 demonstrate motion responses for various time durations. Figure 8 compares pitch response in different durations; it was found that pitch amplitude varied significantly at the beginning of towing operation (before 600 s). After 1 h, however, pitch amplitude varied periodically. It can be clearly seen from Figure 9 that heave amplitude changed irregularly at early towing stages (before 600 s) and, after 1 h, heave change tended to be regular.

Table 4. Heave at different simulation times.

Drift/m	Speed/kn	STD			Mean/m			Normalized Max		
		1 h	3 h	Error	1 h	3 h	Error	1 h	3 h	Error
11.5 m	3 kn	0.022	0.022	1.25%	0.017	0.017	0.10%	2.635	2.934	10.20%
11.5 m	4 kn	0.025	0.026	2.53%	0.017	0.017	0.13%	2.723	2.816	3.29%
11.5 m	5 kn	0.031	0.033	6.17%	0.017	0.017	0.07%	2.807	2.935	4.36%
11.5 m	6 kn	0.043	0.049	12.43%	0.017	0.017	0.27%	2.880	2.916	1.24%
12.5 m	3 kn	0.020	0.020	0.49%	−0.011	−0.011	0.04%	2.635	2.749	4.12%
12.5 m	4 kn	0.022	0.023	2.08%	−0.011	−0.011	0.00%	2.660	2.876	7.51%
12.5 m	5 kn	0.026	0.028	5.24%	−0.011	−0.011	0.05%	2.837	2.965	4.30%
12.5 m	6 kn	0.034	0.039	11.09%	−0.011	−0.011	0.00%	3.033	2.952	2.76%
13.5 m	3 kn	0.034	0.034	0.33%	−0.039	−0.039	0.05%	2.068	2.221	6.88%
13.5 m	4 kn	0.035	0.035	0.44%	−0.039	−0.039	0.05%	2.264	2.447	7.47%
13.5 m	5 kn	0.037	0.037	1.00%	−0.039	−0.039	0.04%	2.463	2.599	5.23%
13.5 m	6 kn	0.041	0.044	7.01%	−0.039	−0.039	0.04%	2.585	2.795	7.50%

Table 5. Pitch at different simulation times.

Drift/m	Speed/kn	STD			Mean/deg			Normalized Max		
		1 h	3 h	Error	1 h	3 h	Error	1 h	3 h	Error
11.5 m	3 kn	0.355	0.371	4.21%	0.023	0.024	5.41%	2.818	2.736	2.96%
11.5 m	4 kn	0.420	0.431	2.56%	0.037	0.040	7.47%	2.915	3.273	10.94%
11.5 m	5 kn	0.438	0.447	1.95%	0.055	0.061	9.53%	3.422	3.343	2.38%
11.5 m	6 kn	0.427	0.424	0.73%	0.075	0.084	11.10%	2.877	3.276	12.18%
12.5 m	3 kn	0.367	0.383	4.16%	0.026	0.028	6.51%	2.716	2.724	0.29%
12.5 m	4 kn	0.412	0.423	2.59%	0.044	0.047	7.45%	3.078	3.289	6.41%
12.5 m	5 kn	0.430	0.442	2.74%	0.064	0.072	10.33%	3.653	3.536	3.31%
12.5 m	6 kn	0.429	0.431	0.55%	0.088	0.099	11.43%	2.867	3.183	9.93%
13.5 m	3 kn	0.370	0.384	3.75%	0.030	0.032	5.66%	2.718	3.043	10.70%
13.5 m	4 kn	0.406	0.418	2.72%	0.050	0.055	8.86%	3.127	3.398	7.96%
13.5 m	5 kn	0.432	0.449	3.88%	0.073	0.082	11.06%	3.560	3.402	4.66%
13.5 m	6 kn	0.450	0.454	0.90%	0.100	0.115	13.15%	2.985	3.211	7.06%

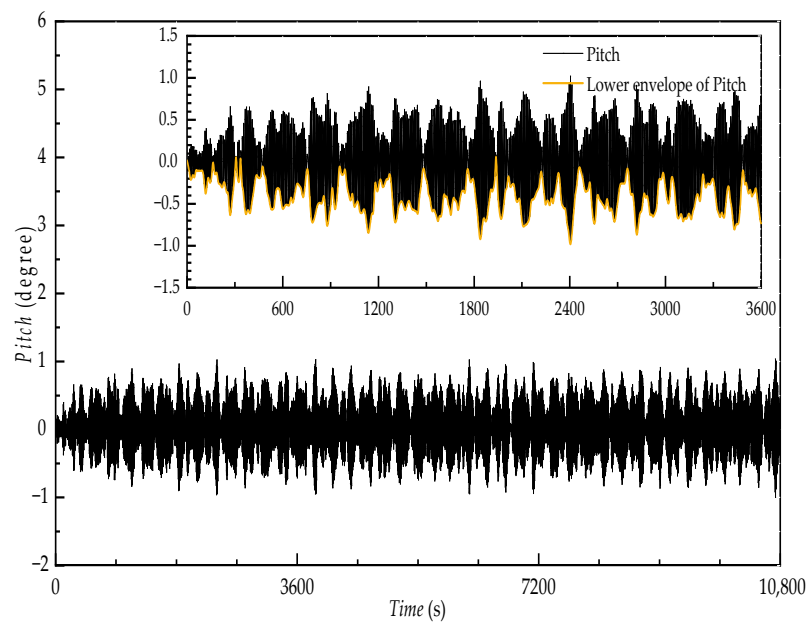


Figure 8. Pitch in 3 h duration.

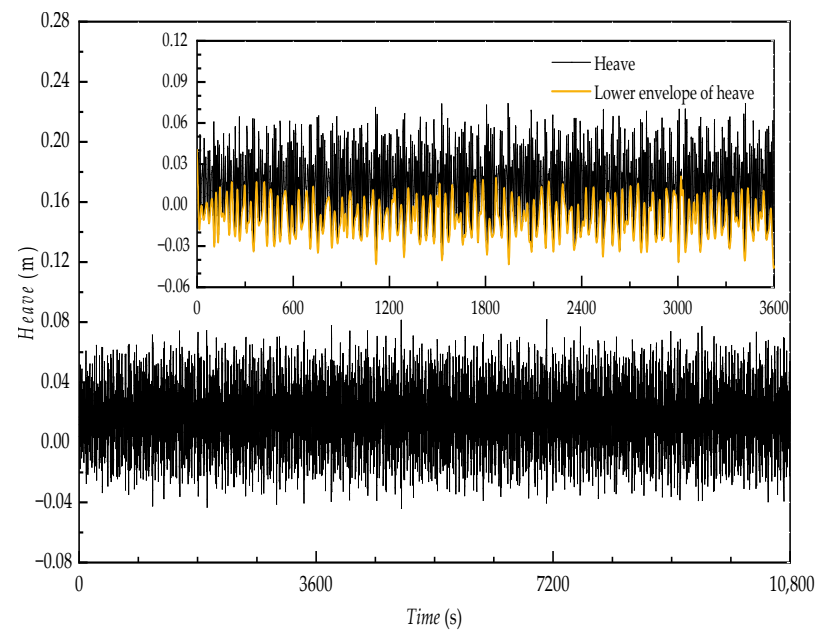


Figure 9. Heave in 3-h duration.

4.2.1. Drift Depth and Towing Speed

Because of the large size of the caisson, its wet surface and water plane could change significantly under violent heave and pitch motions. Four towing speeds and three drift conditions were studied to compare cable tension, heave, and pitch. It is noteworthy that the above three drift depths were greater than those for self-weight balancing and, therefore, ballast weight was applied. It should also be kept in mind that ballast weight was assumed to be placed at the caisson gravity center.

Dynamic response analyses for various drift depths and towing speeds were performed for a towrope length of 100 m. Figure 10 shows the normalized maximums of heave motion and pitch angle. Figure 11 presents bar charts of the *STD* of caisson responses. Figure 12 illustrates towrope tension variation during towing.

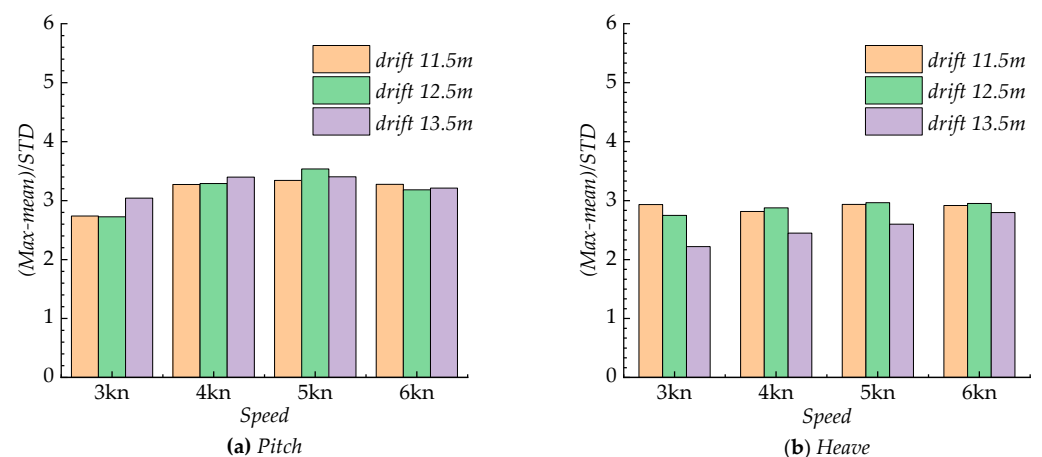


Figure 10. Normalized maximums for different drift depths and towing speeds.

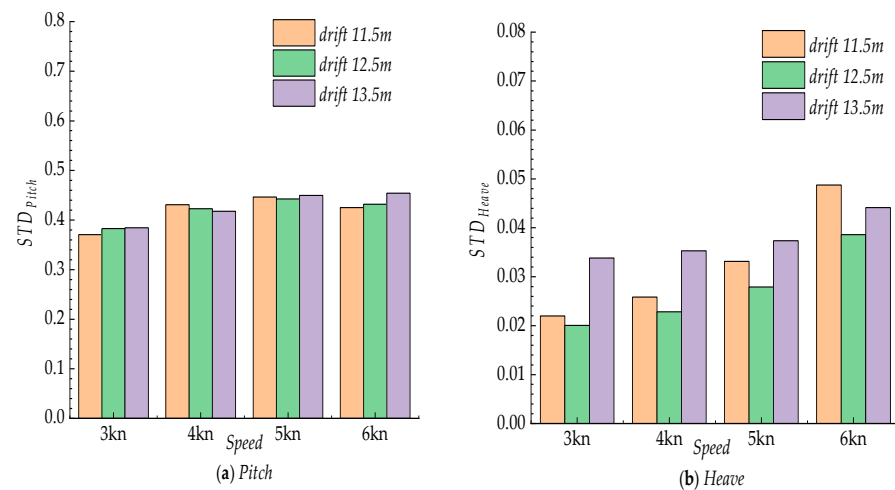


Figure 11. STD of dynamic responses for different drift depths and towing speeds.

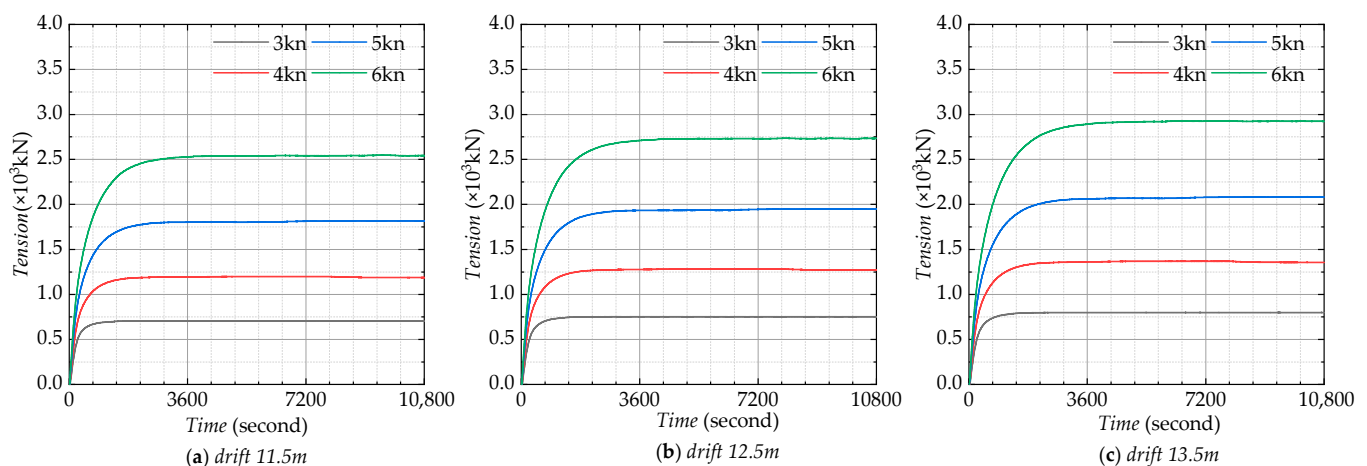


Figure 12. Towrope tension at different drift depths and towing speeds.

As can be seen from Figure 10a, at a constant towing speed, the normalized maximums of pitch angle barely changed (around 2.6–3.2) when increasing drift depth, especially at a towing speed of 6 kn. Additionally, at constant drift depth, normalized maximums of pitch angle slightly fluctuated when increasing towing speed. Figure 10b reveals that, at drift depths of less than 13.5 m, normalized maximums of heave motion barely changed when increasing towing speed. However, at a drift depth of 13.5 m, normalized maximum of heave was less than the former one and increased with towing speed.

As can be seen in Figure 11a, towing speed and drift depth had insignificant effects on pitch angle STD because the caisson water plane was constant no matter the drift depth changes. So, large wet surface areas could have small effects on pitch motion [18]. As can be seen in the bars presented in Figure 11b, heave motion fluctuations by increasing towing speed were significant. Additionally, at a drift depth of 12.5 m and a constant towing speed, heave motion STD was smaller than those of the other two conditions.

Towrope tension is another key index for the measurement of towing safety. Towrope tension variations at various towing speeds and drift depths were evaluated, and the obtained results are shown in Figure 12. Towrope tension tended to remain constant after towing for about 1 h. By increasing towing speed, the time required for stabilization was increased. According to the towrope tension [28] calculation equation, flow surface areas and relative velocity greatly influenced the towrope. Therefore, an increase of towing speed increased the towrope tension.

4.2.2. Drift Depth and Towrope Length

The towrope should have adequate length to guarantee that the caisson would not collide with the tugboat during the whole towing process. Taking account of the length of the caisson and the tugboat, as well as the towing speed, the towrope length adopted in this research is 100 m, 150 m, and 200 m. Dynamic responses were analyzed for three towrope lengths and two drift depths at a constant towing speed of 3 knots.

Normalized maximums for various depths and towrope lengths in pitch and heave are shown in Figure 13. It could be easily concluded that variations in maximum pitch angle (around 3.2–3.6) were not greatly affected by towrope length by comparing the normalized maximum of the pitch angle with different towrope lengths at a given drift depth. However, the heave motion peak was influenced by towrope length. As seen from Figure 14a, pitch angle *STD* was barely changed with towrope length, indicating that the pitch angle fluctuation was hardly influenced by towrope length. Figure 14b reveals that towrope length had unobvious effects on heave response fluctuation. Therefore, it can be easily concluded that towrope length had a limited effect on the normalized maximum values and *STD*s of heave and pitch.

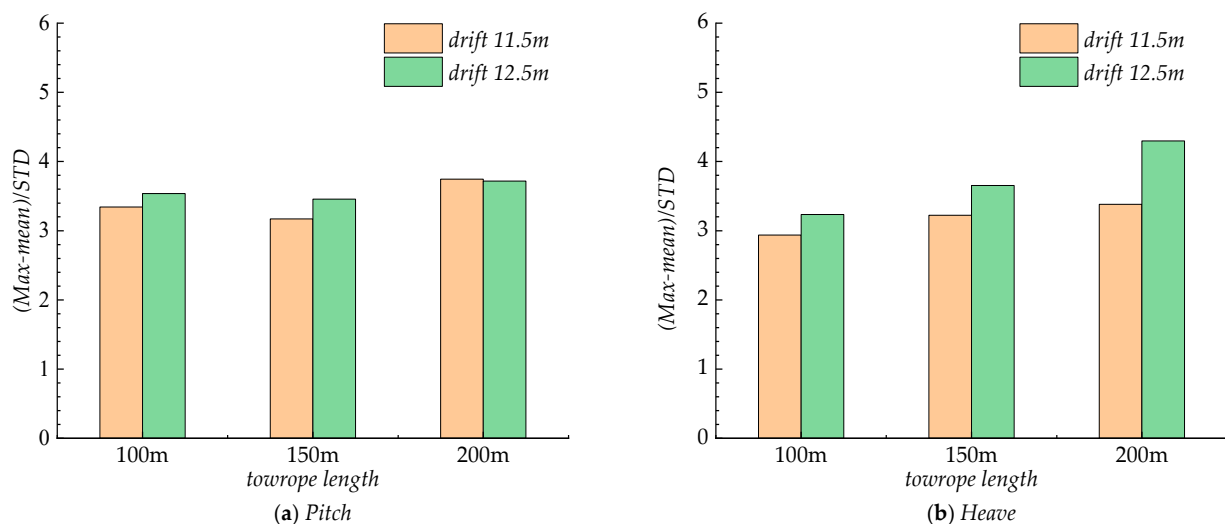


Figure 13. Normalized maximums for different drift depths and towrope lengths.

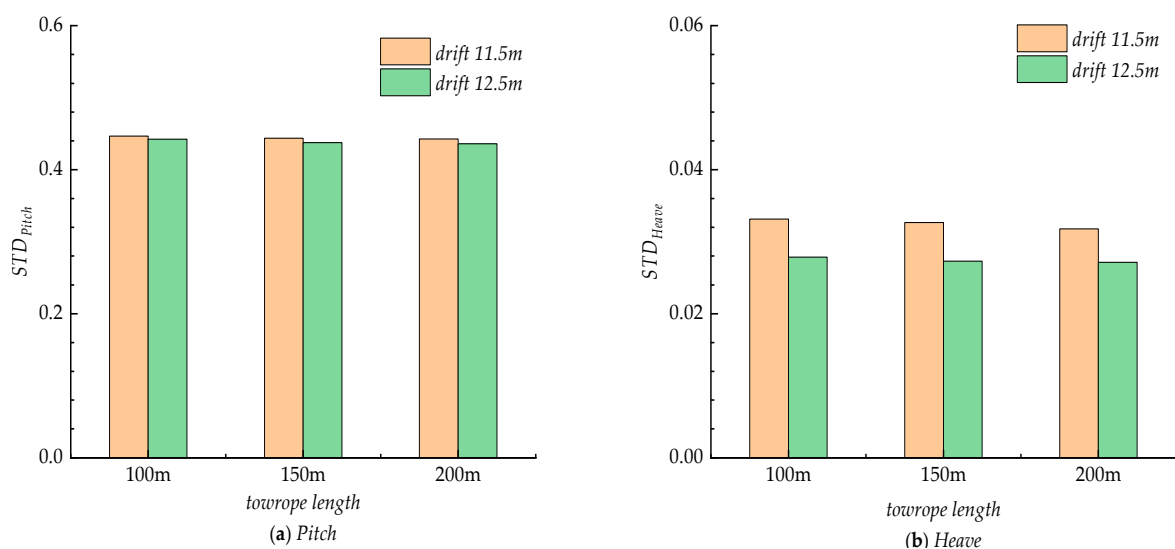


Figure 14. *STD* of dynamic responses at different drift depths and towrope lengths.

Figure 15 illustrates the towrope tension time domain curves for various towrope lengths and drift depths. Towrope tension was increased from 0 to a maximum value, then tended to remain constant. This constant value was similar at given drift depths and towing speeds, regardless of towrope length, which totally complied with the proposed calculation equation (CCS, 2011). However, by increasing the length of the towrope, tension was increased faster at the beginning of towing (less than 1 h).

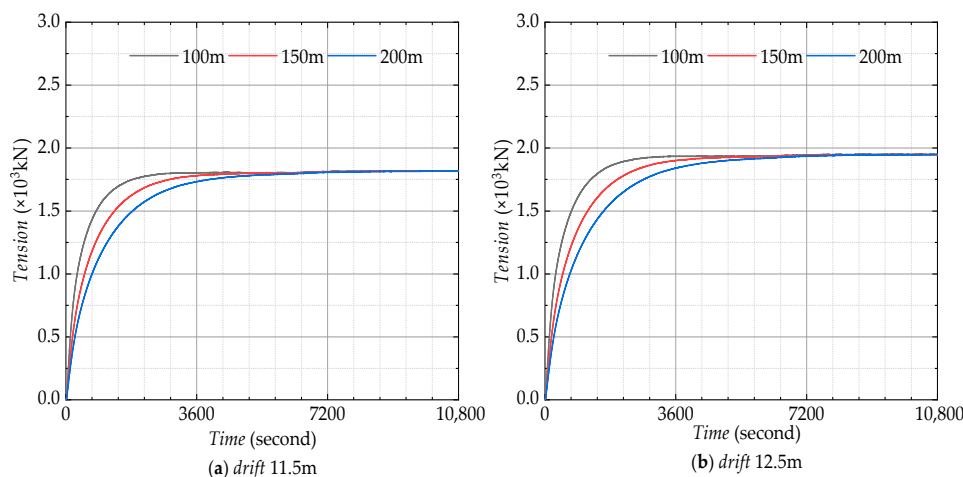


Figure 15. Towrope tension at different drift depths and towrope lengths.

4.3. Estimated of CO₂ Emissions

Currently, the power of general tugboats is in the range of 4000–5000 kW. In the current work, we assumed that the tugboat worked with a constant power of 4500 kW and towing distance was 30 nautical miles. Therefore, the actual number of tugboats required for various working conditions was calculated based on towrope tension. Additionally, CO₂ emissions calculated by the equation are shown in Table 6.

Table 6. Calculation of CO₂ emissions.

Drift/m	Speed/kn	Tensions/KN	Number of Tugboats	MCR	LF	A	EF	Emissions of CO ₂ /kg
11.5	3	704.5426	1	4500	0.68	10	0.744	22,766.4
11.5	4	1187.94	2	9000	0.68	7.5	0.744	34,149.6
11.5	5	1816.56	3	13,500	0.68	6	0.744	40,979.52
11.5	6	2541.9	3	13,500	0.68	5	0.744	34,149.6
12.5	3	751.4154	1	4500	0.68	10	0.744	22,766.4
12.5	4	1272.13	2	9000	0.68	7.5	0.744	34,149.6
12.5	5	1947.65	3	13,500	0.68	6	0.744	40,979.52
12.5	6	2734.05	3	13,500	0.68	5	0.744	34,149.6
13.5	3	799.2422	1	4500	0.68	10	0.744	22,766.4
13.5	4	1356.29	2	9000	0.68	7.5	0.744	34,149.6
13.5	5	2083.59	3	13,500	0.68	6	0.744	40,979.52
13.5	6	2922.2	3	13,500	0.68	5	0.744	34,149.6

It can be seen from the data provided in Table 6 that the number of tugboats required for the mentioned working conditions was 1 to 3. Due to relatively small differences in draft changes for several different working conditions, draft did not affect the number of required tugboats. Comparing CO₂ emissions for the same draft at different speeds showed that, when speed was 3 kn, only one tugboat could afford the project. Although towing time was 10 h, CO₂ emissions were only 2766.4 kg. At the speed of 4 kn, however, one less tug was used than at a speed of 6kn, although it took 2.5 h longer to tow. Surprisingly, CO₂ emissions of both cases were equal to 34,149.6 kg. At the speed of 5 kn, CO₂ emissions were the largest and equal to 40,979.52 kg. In addition, from an energy point of view, by

the increase of CO₂ emissions, more energy was actually required for the above conditions. That is to say, at the speed of 5 kn, the highest amount of energy was consumed.

5. Conclusions

The towing of caissons with bulkheads inside was studied in the current work. The towing system consisted of the caisson, a towrope, and tugboats. Wet towing was designed as an economical and wieldy transportation method. A numerical evaluation was performed, which provided a new method to assess the feasibility of the developed method, and the following conclusions were drawn.

Drifts and towing speeds had little effect on pitch response regardless of normalized maximums and their fluctuations, while deeper drifts result in higher heave maximums when the towing speed is given. Drifts also significantly affected heave fluctuations. At drift depth of 12.5 m, *STD* was smaller than those of the other two cases. At a certain drift, towing speed more significantly affected pitch fluctuations compared to heave fluctuations. Once a stable state was obtained for the towing process, towrope tensions were determined by towing speeds and drifts. Towrope length was found to have an insignificant effect on heave and pitch responses. However, it could affect the speed of achieving a stable state for towrope tension. Meanwhile, CO₂ emissions were mainly affected by towing speed. Above all, the optimum towing plan for the project was a drift depth of 12.5 m, a towing speed of 3 kn, and a towrope length of 200 m.

Author Contributions: H.G. contributed to the conception of the study and carried numerical simulations; H.W. contributed significantly to analysis and manuscript preparation; Q.Z. helped perform the analysis with constructive discussions; W.F. helped the analysis with constructive discussions; J.C. carried out numerical simulations. All authors have read and agreed to the published version of the manuscript.

Funding: This research received no external funding.

Institutional Review Board Statement: This study do not require ethical approval.

Informed Consent Statement: Informed consent was obtained from all subjects involved in the study.

Data Availability Statement: Data available on request due to restrictions e.g., privacy or ethical. The data presented in this study are available on request from the corresponding author. The data are not publicly available due to the Chinese law.

Conflicts of Interest: We declare no conflict of interest.

References

1. Wang, Y.; Miao, W.; Ding, Q.; Li, C.; Xiang, B. Numerical investigations on control strategies of wake deviation for large wind turbines in an offshore wind farm. *Ocean Eng.* **2019**, *173*, 794–801. [[CrossRef](#)]
2. Algaze, G. *Ancient Mesopotamia at the Dawn of Civilization: The Evolution of an Urban Landscape*; The University of Chicago Press: Chicago, IL, USA, 2008.
3. Kim, B.; Kim, T.W. Scheduling and cost estimation simulation for transport and installation of floating hybrid generator platform. *Renew. Energy* **2017**, *111*, 131–146. [[CrossRef](#)]
4. Kim, B.; Kim, T.W. Monte Carlo simulation for offshore transportation. *Ocean Eng.* **2017**, *129*, 177–190. [[CrossRef](#)]
5. Sinibaldi, M.; Bulian, G. Towing simulation in wind through a nonlinear 4-dof model: Bifurcation analysis and occurrence of fishtailing. *Ocean Eng.* **2014**, *88*, 366–392. [[CrossRef](#)]
6. Marine Accident Investigation Branch (MAIB). *Report on the Investigation of the Loss of the Tug Flying Phantom While Towing Red Jasmine on the River Clyde on 19 December 2007. Resulting in 3 Fatalities and 1 Injury*; Report No. 17/2008; Marine Accident Investigation Branch (MAIB): Southampton, UK, 2008. Available online: <https://assets.publishing.service.gov.uk/media/547c7010ed915d4c0d000073/FlyingPhantom.pdf> (accessed on 4 January 2021).
7. Transportation Safety Board of Canada (TSB). *Marine Investigation Report M09W0141. Tug Girding and Capsizing. Tug North Arm Venture While Towing the Barge North Arm Express, Entrance to the Sechelt Rapids, British Columbia, 19 July 2009*; Transportation Safety Board of Canada (TSB): Gatineau, QC, Canada, 2009. Available online: <https://www.bst-tsb.gc.ca/eng/rappports-reports/marine/2009/m09w0141/m09w0141.pdf> (accessed on 4 January 2021).
8. Lyng, I.; Andreassen, D.; Fiksdal, G.; Loken, G.; Skolvoy, Y.; Pettersen, T. *The Loss of the Bourbon Dolphin on 12 April 2007*; Official Norwegian Reports; Government Administration Services: Oslo, Norway, 2008; Volume 8, ISBN 987-82-583-0965-6.

9. Berg, P. A Discussion of Technical Challenges and Operational Limits for Towing Operations. Master's Thesis, Norwegian University of Science and Technology, Trondheim, Norway, 2017.
10. Berbitsas, M.M.; Kekridis, N.S. Nonlinear Stability Analysis of Ship Towed by Elastic Rope. *J. Ship Res.* **1986**, *30*, 136–146.
11. Bernitsas, M.M.; Kekridis, N.S. Simulation and Stability of Ship Towing. *Int. Shipbuild. Prog.* **1985**, *32*, 112–123. [[CrossRef](#)]
12. Fitriadhy, A.; Yasukawa, H.; Koh, K.K. Course stability of a ship towing system in wind. *Ocean Eng.* **2013**, *64*, 135–145. [[CrossRef](#)]
13. Fitriadhy, A.; Yasukawa, H. Course stability of a ship towing system. *Ship Technol. Res. Schiffstechnik.* **2011**, *58*, 4–23. [[CrossRef](#)]
14. Jurewicz, J.M. Design and Construction of an Offshore Floating Nuclear Power Plant. Doctoral Dissertation, Massachusetts Institute of Technology, Cambridge, MA, USA, 2015.
15. Kang, W.; Zhang, C.; Yu, J.X. Stochastic extreme motion analysis of jack-up responses during wet towing. *Ocean Eng.* **2016**, *111*, 56–66. [[CrossRef](#)]
16. Zhao, Z.; Tang, Y.; Wu, Z.; Li, Y.; Wang, Z. Towing Analysis of Multi-Cylinder Platform for Offshore Marginal Oil Field Development. In Proceedings of the ASME 2016 35th International Conference on Ocean, Offshore and Arctic Engineering, Busan, Korea, 19–24 June 2016.
17. Ding, H.; Han, Y.; Le, C.; Zhang, P. Dynamic analysis of a floating wind turbine in wet tows based on multi-body dynamics. *J. Renew. Sustain. Energy* **2017**, *9*, 033104. [[CrossRef](#)]
18. Zhang, P.; Peng, Y.; Ding, H.; Hu, R.; Shi, J. Numerical analysis of offshore integrated meteorological mast for wind farms during wet towing transportation. *Ocean Eng.* **2019**, *188*, 106271. [[CrossRef](#)]
19. JIAN FENG SLING CO., LTD. Available online: http://www.jian-feng.com/page85.html?article_id=9 (accessed on 13 December 2020).
20. Rawson, K.J.; Tupper, E.C. *Basic Ship Theory*; Longman: London, UK, 2001.
21. Lee, S.; Hong, C. Study on the course stability of very large vessels in shallow water using CFD. *Ocean Eng.* **2017**, *145*, 395–405. [[CrossRef](#)]
22. Liu, Y.; Zou, Z.; Zou, L.; Fan, S. Cfd-based numerical simulation of pure sway tests in shallow water towing tank. *Ocean Eng.* **2019**, *189*, 106311. [[CrossRef](#)]
23. Jin, Y.; Duffy, J.; Chai, S.; Chin, C.; Bose, N. URANS study of scale effects on hydrodynamic manoeuvring coefficients of KVLCC2. *Ocean Eng.* **2016**, *118*, 93–106. [[CrossRef](#)]
24. He, R.; Zhang, Z.Z.; Wang, X.Z.; Feng, D.K. Numerical simulation of the ship bottom interaction DTC container carrier for different keel clearance in pure sway motion. In Proceedings of the 4th International Conference on Ship Manoeuvring in Shallow and Confined Water (MASHCON): Ship-Bottom interaction, Hamburg, Germany, 23–25 May 2016; pp. 65–72.
25. Tang, S. Flow Friction of Pile and Pile Group and Its Application on the Tidal Numerical Modelling. Doctoral Dissertation, Dalian University of Technology, Dalian, China, 2002.
26. Jürgen, W. *Handbook of Terminal Planning*, 2nd ed.; Springer: Suderburg, Germany, 2011.
27. Karimirad, M.; Moan, T. Wave-and wind-induced dynamic response of a spar-type offshore wind turbine. *J. Waterw. Port Coast. Ocean Eng.* **2012**, *138*, 9–20. [[CrossRef](#)]
28. CCS. *Guidelines for Towing at Sea*; CCS: Beijing, China, 2011.